Comparison of three different techniques for gas-liquid mass transfer visualization

Feishi Xu, Gilles Hébrard, Nicolas Dietrich

COMPARISON OF THREE DIFFERENT TECHNIQUES FOR GAS-LIQUID MASS TRANSFER VISUALIZATION

Feishi XU, Gilles HEBRARD and Nicolas DIETRICH*

Toulouse Biotechnology Institute (TBI), Université de Toulouse, CNRS, INRA, INSA, 135 Avenue de Rangueil, 31077 Toulouse, France,

(Corresponding author's e-mail: dietrich@insa-toulouse.fr)

Abstract

In this article three different techniques for visualizing gas-liquid mass transfer are reviewed according to their applications in air-water systems. The three techniques are: Planar Laser Induced Fluorescence (PLIF with the use of fluorescent resorufin), PLIF with Inhibition (PLIF-I with the use of a ruthenium complex), and a colorimetric technique (using a redox reaction with the pink-colored dye resorufin). For comparison purpose, the three techniques were conducted in the same experimental set-up to characterize the local oxygen mass transfer from a single air bubble (with equivalent diameter ~1 mm) rising in water. This paper rigorously compares these three techniques and aims to point out their advantages and limitations. The comparison was divided into two parts: the visualization and the quantification of the mass transfer. The discussion focused on the image quality, the required equipment, and the accuracy of the quantification results including the mass flux, the diffusion coefficient and the mass transfer coefficient. A guideline was provided for choosing the technique that most accurately visualizes and characterizes the local mass transfer in gas-liquid systems.

Keywords: Bubble, Gas-liquid, Mass transfer, Fluorescence, Colorimetric reaction, Fluorescence quenching

1. INTRODUCTION

Most of the modern visualization techniques for gas-liquid mass transfer are based on the addition of an indicator (fluorescent dye or colorimetric dye) into the liquid phase which can be captured by optical instrument [1,2]. Compared with the probe technique [3,4], the visualization techniques have the advantages of no flow disturbance, quick response time and high visual resolution, and the capacity to elucidate the profile near the gas-liquid interface despite its limited thickness [5]. They can also be easily combined with other optical methods that can provide simultaneous measurements of flow velocity and temperature [6].

According to the principle of these techniques, the main visualization techniques can be classified as the traditional fluorescence technique (i.e. PLIF: Planar Laser Induced Fluorescence), the inhibited fluorescence technique (i.e. PLIF-I: Planar Laser Induced Fluorescence with Inhibition), and the colorimetric technique (with a dissolved gas-sensitive dye).

1.1 Traditional fluorescence technique

Planar Laser-induced fluorescence technique (PLIF) was proposed in the late 1960s and was applied to gas combustion process for studying the heat transfer at early stage [7]. Then PLIF has been rapidly extended to study the mixing by the dispersion of fluorescent tracers in liquid and gaseous flows. As a traditional fluorescence technique, the measurement is based on the linearity between the fluorescence intensity and the concentration of fluorophore in the weak excitation regime [8]. Under weak excitation condition (excitation intensity I much smaller than the saturation intensity of the dye), the relationship between fluorescence level F and local concentration of the dye C_{dye} has a simplified relationship:

$$F \propto I \cdot C_{dye} \tag{1}$$

where *I* can be assumed as constant [9,10]. Thus, using a multi-pixel light sensitive sensor (CMOS or CCD cameras), one can record the fluorescence signal and thus determine the corresponding instantaneous concentration field of the dye.

1.2 Inhibited fluorescence technique

The traditional PLIF requires the transported species itself play as a role of fluorophore which is difficult to realize for most gas-liquid species. Therefore, several variants of PLIF technique appears with the respective personalized name: PLIF-I (PLIF with Inhibition [11]), 2T-LIF (Two-tracer LIF [12]), LIF/HPTS [13], BPLIF (Blocked PLI, [14]), I^{R}_{PH}-PLIF (Ratiometric pH-sensitive-inhibited [15]), DeLIF (Dual Emission LIF, [16]), etc. Different from traditional PLIF techniques, the fluorophore is here pre-mixed homogeneously into the liquid. Fluorescence of this kind of dye under monochromatic excitation can be affected by the presence of a flow-passive scalar (e.g. concentration of a chemical species, pH value, temperature etc.) (Figure 1). The value of this scalar can be deduced from the variation of fluorescence intensity once a previous calibration is done that fluorescence intensities are measured for several preset values of the scalar.

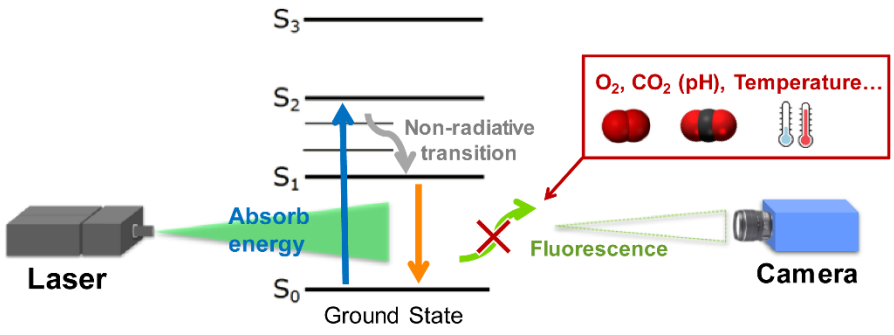

Figure 1 Schematic description of the principle of variant LIF techniques by Jablonski diagram.

A representative example of the inhibited fluorescence technique (noted as PLIF-I afterward) is based on the quenching phenomena of the fluorescence [17]. In a

quenching experiment, the ability of some molecules called “quenchers” to inhibit the fluorescence is considered which can reduce the fluorescence lifetime of the fluorophore. Regarding the fluorescence lifetime is proportional to fluorescence intensity, the dynamic quenching process is expressed as the Stern-Volmer relationship:

$$\frac{I_Q}{I_0} = \frac{1}{1+K_{SV}Q} \quad (2)$$

where K_{sv} is the Stern-Volmer constant, and I_Q and I_0 the fluorescence intensities in the presence and absence of quencher, respectively. The parameters I_0 and K_{sv} of the Stern-Volmer equation can be easily determined by a calibration process by measuring several I_Q values under different preset concentration of quenchers.

The combination of fluorescence intensity measurements with the effect of fluorescence quenching for gas concentration measurements in liquids was first introduced by Vaughn and Weber [18]. As oxygen has been known as an excellent quencher, Wolff et al. [19] introduced primarily PLIF-I technique to visualize O_2 concentration near a gas-liquid interface. Many following researchers [5,20–22] have continued to work on the same subject by studying the absorption of O_2.

1.3 Colorimetric technique

The third category of techniques calls the colorimetric technique. It is based on the oxidation and reduction reactions by which the concentration of the target species can be deduced from the change in color of a dissolved dye. Among the literature about colorimetric methods, methylene blue [23], resazurin [24] and leuco-indigo carmine [25] were mainly applied as dyes to investigate mass transfer and concentration fields. The method used in this study was the colorimetric technique proposed by Dietrich et al. [24]. Resazurin (CAS 62758-13-8, molecular mass: 229.19 $g \cdot mol^{-1}$) was chosen as the dye which reacts with oxygen in the presence of sodium hydroxide (NaOH) and glucose solution.

When resazurin dissolves in water (blue and not fluorescent), it is reduced to resorufin (pink and highly fluorescent). Then reversible reduction-oxidation occurs between resorufin and dihydroresorufin (colorless and not fluorescent). Since the oxidation reaction is quasi-instantaneous and the reduction reaction is slow (few minutes), it is possible to visualize the pink colored field under a white light source. The oxidation reaction can be expressed as follows:

$$O_2 + 2 \times \text{dihydroresorufin} \rightarrow 2 \times \text{resorufin} + 2 \times H_2O \quad (3)$$

When there is sufficient resazurin to react with all the transferred oxygen, the number of moles of dissolved oxygen can be deduced from the number of moles of resazurin, as

$$n_{O_2,transferred} = n_{O_2,reacted} = \frac{n_{resazurin}}{2} \quad (4)$$

1.4 Application of the visualization techniques to gas-liquid systems

All the above three techniques have been applied to a wide variety of gas-liquid contacting conditions, including bubbly flows, flows across the planar interface and Taylor flows / confined flows.

Among several industrial processes (e.g. bubble column reactor, stirred tank, etc.), the gas phase usually appears as a form of bubble swarms or isolated bubble because of their high interfacial area for gas-liquid mass transfer [26]. The visualization techniques provides an efficient tool to characterize the transferring process for different type of gas: air [11,27–29], oxygen [20,30] and carbon dioxide [1,31,32].

A series of representative researches have been conducted which apply visualization techniques to investigate mass transfer from bubbles in recent decades. Bork et al. [33] investigated the impact of local phenomena on mass transfer from bubbles according to the bubble diameters and the liquid viscosities as variation parameters by using the quenching reaction with a ruthenium complex. Stöhr et al. [31] visualized the

gas-liquid mass transfer and wake structure of rising bubbles using acid-based PLIF. The resulting PLIF image sequences revealed the evolution of characteristic patterns in the near and far wake of the bubbles and further allowed the estimation of bubble size and rise velocity. Kück et al. [30,34] investigated the impact of local phenomena on mass transfer from single free-rising gas bubbles with and without a superimposed chemical reaction using PLIF and PIV (Particle Image Velocimetry). Jimenez et al. [11] worked on the mass transfer of an ellipsoidal bubble, also indicating the influence of the bubble diameter and the liquid composition (glycerol, salt, glucose) on the flux density by PLIF-I technique. Based on a similar configuration, Dietrich et al. [35] captured pictures of the concentration field at micro-scale in the laminar bubble wake, which enabled the gas-liquid diffusivity to be accurately evaluated in a very short time of around one second. Saito and Toriu [36] used experimental results from highly precise measurements of bubble volume to clarify the instantaneous mass-transfer coefficients of a zigzag CO_2 bubble. The zigzag motion and surface oscillation, as well as the CO_2 dissolution (mass transfer) process from the bubble to the surrounding liquid, were simultaneously visualized by using two high-speed cameras and mirrors with the PLIF with a PH sensitive dye HPTS. Based on a similar configuration, Huang and Saito [13,37,38] discussed the influences of gas-liquid interface contamination on the bubble motions, bubble wake patterns, and the mass transfer process, through the reconstruction of three-dimensional bubble wakes in purified water and contaminated water. Timmermann et al. [39] investigated the influence of bubble collisions on the local concentration field at well-defined conditions and that of a superimposed sodium sulfite reaction on the concentration field after bouncing. Using a high-speed PIV/LIF system combined with direct visualization, the local and temporal evolution of the CO_2 chemisorption in aqueous NaOH solution in a cylindrical bubble column was investigated [12] and compared with simulation results [40]. Focusing on the convective mass transfer contribution, Kong et al. [41] used fluorescein as a dye to study the case of a millimetric CO_2

bubble suspended under a substrate and dissolved in pure liquid water. Based on the reduction of the colorimetric indicator (resorufin) in presence of oxygen, Dietrich and Hébrard [42] estimated the liquid-side mass transfer coefficient around a freely rising bubble and the result proved that the colorimetric technique had the potential to provide new, detailed insight into the spatiotemporal dynamics of the mass transfer of rising gas bubbles. More recently, the PLIF-I technique was applied to a non-Newtonian fluid to study the impact of fluid properties on the mass transfer coefficient [43,44].

These studies from the literature show that the techniques using soluble fluorescent or colorimetric dyes and optical equipment are efficient to visualize the local mass transfer from a bubble with high resolution.

Taylor flows have been widely studied because of their performance in terms of both heat and mass transfer, and their regularity, stability, and operability in a broad operating domain. Dietrich et al. [24] first proposed the colorimetric technique (with resorufin) to investigate mass-transfer in Taylor flow. Gray value maps were converted to equivalent oxygen concentrations and a mass transfer model was established, presenting the local characterization of gas-liquid mass transfer. In addition, Yang et al. [45] considered the possibility of enhancing gas-liquid mass transfer by this oxygen colorimetric reaction. Once the kinetic constant and diffusion coefficients had been determined by colorimetric methods, the Hatta number and enhancement factor were deduced, and there was no enhancement of the gas-liquid mass transfer by this extremely fast oxygen reaction. As for the non-invasive and instantaneous advantages, Yang et al. [46] further investigated the mass transfer contribution of the bubble formation stage to the overall process. The liquid side mass transfer coefficients at the moment immediately after the pinch-off stage were obtained and founded bigger than in the flowing stage, which demonstrated that the contribution of the bubble formation stage to overall mass transfer was reasonably large [47,48]. Furthermore, Yang et al. [49] studied the mass transfer intensification in

a square meandering channel. A comparison between methylene blue and resazurin systems used in a helically-coiled tube showed better performance by the resazurin system due to the larger difference of time constants in terms of oxidation and reduction processes [50]. Krieger et al. [25] utilized leuco-indigo carmine to visualize local mass transfer and concentration distributions, also investigating chemical selectivity because of the existence of the anionic radical intermediate state. As overlap of three different indigo carmine colors could result in multiple colors, the isolation of each indigo carmine in the calibration procedure was achieved by an imaging processing technique and UV/Vis spectrometry methods. In a more complicated system for the combined mass transfer process and chemical reaction, Kastens et al. [51] reported oxygen concentration fields and wake structures around a Taylor bubble and compared the wake structures they observed with that obtained using the PIV-LIF technique, while Butler et al. [52,53] first investigated the mass transfer of a Taylor oxygen bubble by means of the PLIF-I technique and deduced the oxygen concentration based on Stern-Volmer relations using the ruthenium fluorescence intensities. By employing two groups of PLIF-I images, namely with O_2 and N_2 as the gas phase, they successfully corrected the light scattered by the gas phase in O_2 images by means of N_2 images taken as references. They separated mass transfer coefficients for film to bubble, film to slug and bubble cap to slug, with a good precision.

In confined 2D Hele-Shaw cells, bubbles were largely flattened by narrow gaps and confined to move with only two degrees of freedom. Bouche et al. [27] used two fluorescent dyes (i.e., Fluorescein Sodium and Rhodamine WT) to remove the light reflections caused by the gas interface, and Alméras et al. [54] further analyzed the fluctuations of concentration. Roudet et al. [55] estimated the total mass transfer rate using the Sherwood number and Péclet number and compared the mass transfer rate in the films with total mass transfer. Felis et al. [56,57] investigated the oxygen mass transfer and local oxygen concentration around a rising bubble and compared the

equivalent oxygen concentration obtained by resazurin with that given by Cu/O_2 complexes.

Several excellent reviews have been made focusing on fluorescence techniques [8,58], however, they mixed the traditional PLIF techniques with inhibited PLIF techniques even though they are theoretically different. For comparison purpose, the experiments of the work presented here were conducted on the same experimental setup to characterize the local mass transfer and the diffusion around a single air bubble rising in water by using PLIF (with fluorescent resorufin), PLIF-I (with ruthenium complex), and colorimetric techniques (with pink resorufin).

2. MATERIALS AND METHOD

2.1 Experimental setup

The experimental setup, depicted in Figure 2, was based on a dual camera system [20]. The glass column made of transparant PMMA (Poly (methyl methacrylate)) had dimensions of 100×100×300 mm^3. A stainless steel needle was inserted into the column through a hole located 20 mm above the bottom of the column. The needle was used for bubble injection, the bubble being pushed out of the tip of the needle when the other side of the needle was connected to a syringe pump (Harvard Apparatus PHD 22/2000 Programmable, USA).

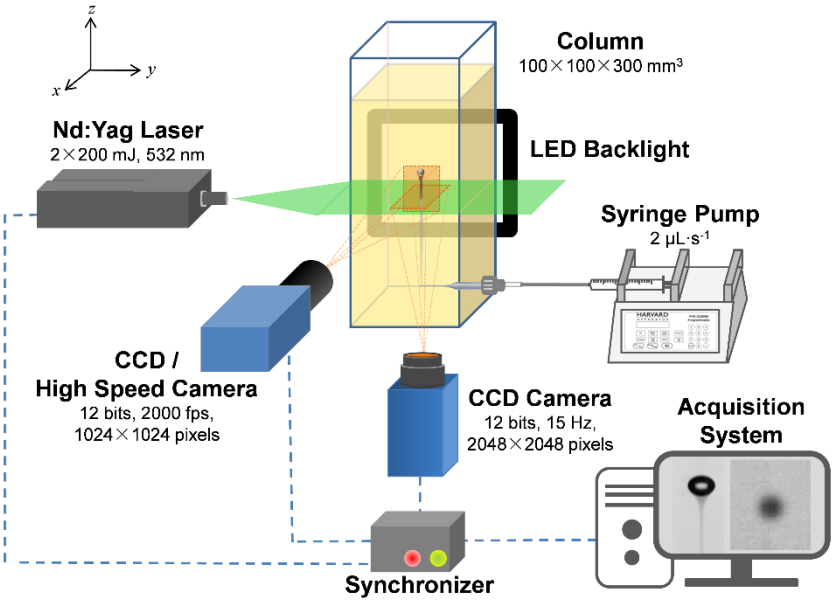

Figure 2 Experimental setup

For laser-based techniques (i.e. PLIF and PLIF-I), a horizontal laser sheet was generated by a Nd:Yag laser (Dantec Dynamics Dualpower 200-15, France) and positioned about 100 mm above the needle. The high-intensity laser (2×200 mJ) emitted light with a wavelength of 532 nm, which enabled the dye to be excited with a frequency of 15 Hz.

When the bubble was rising in the column, the images of the fluorescence in the bubble wake were recorded by a Charge-Coupled Device (CCD) camera (Dantec Dynamics Flowsense CM). The camera was placed under the column and focused on the laser sheet. A microlens (105 mm f/8, Canon) with an extension tube (36 mm) was applied to increase the magnification of the investigated area. The length scale was calibrated with a ruler and image area was about 10 × 10 mm^2 in real distances. A 570 nm high-pass filter was placed in front of the lens to block the laser light. The CCD camera was synchronized with the laser thus 15 images were acquired every second in the forms of 12 bits and 2048×2048 pixels of resolution. For each bubble, the time was set to 0 when the first image containing the transferred mass was taken. A

high-speed camera (Photron SA3, Japan) was placed orthogonally to the first camera, next to one lateral side of the column. It was used to capture the hydrodynamics of the bubble, such as the velocity, shape, and trajectory of the bubble at a rate of 2000 fps. The images were in 8 bit format with a resolution of 1024×1024 pixels. The length scale was calibrated with a ruler and, in real distances, the image area was about 30×30 mm^2. The backlight was provided by a LED lighting board facing the camera.

The images from the two cameras were then transferred to the acquisition system, which consisted of two professional software packages (DynamicStudio 4.0 and Photron Fastcam Viewer 2). They can carry out simple image adjustment such as color filtration, length calibration, etc. It should be noted that the above experimental setup was designed to characterize the mass transfer in the bubble wake. To visualize the mass transfer near the bubble interface, the laser sheet should be positioned vertically and the positions of the two cameras may be switched.

All the experiments were carried out under the controlled conditions, i.e. with the same needle (~ 0.7 mm of inner diameter) and same flow rate (2 $\mu L \cdot s^{-1}$) for bubble injection, at a temperature of 293.15 K and under atmospheric pressure (1 atm). The good reproducibility of the bubble size (~ 1 mm), shape (ellipsoidal) and trajectory (vertical) of the injected bubbles allowed us to assume that each of the individual bubbles examined was identical. The details of the materials and properties of the bubbles in the experiments are given in Table 1.

Table 1 Composition of the fluids and properties of the bubbles for comparison of three techniques

	PLIF-I	**PLIF**	**Colorimetric technique**
Liquid-Gas	Deionized water + Air bubble		
Dye	Ruthenium Complex	Resazurin 100 $mg \cdot L^{-1}$ (+ NaOH 20 $g \cdot L^{-1}$	

	75 mg·L^{-1}	+ Glucose 20 g·L^{-1})
σ [mN·m^{-1}]	72	75
ρ [kg·m^{-3}]	1000	1004
μ [mPa·s]	1.003	1.100
Diameter of bubble	1.25 ± 0.04 mm	
Aspect ratio of bubble	1.13 ± 0.02	
Velocity of bubble	295 ± 10 mm·s^{-1}	
Re	368± 20	

2.2 Oxygen indicator (dye)

In the mass transfer visualization experiments, the oxygen concentration is indicated by different dissolved dyes: ruthenium complex for PLIF-I and resorufin for the colorimetric technique and the PLIF technique.

Ruthenium complex

In this study, a type of ruthenium complex ($C_{36}H_{24}Cl_2N_6Ru{\cdot}xH_2O$, Sigma-Aldrich, USA, CAS: 207802-45-7) is adopted as a fluorescence dye. This dye is easy to dissolve in water and has a large separation between absorption and emission spectra (Stock shift) [30,34]. The fluorescence efficiency has been tested for different concentrations of dye [59] by comparing the difference of the gray levels when dissolved oxygen concentration varies from 0 mg·L^{-1} to 3 mg·L^{-1}. It was found that when the concentration of the dye passes a critical value (~75 mg·L^{-1}), the fluorescence efficiency no longer increases. Thus, the concentration of dye was set at 75 mg·L^{-1} to guarantee fluorescence efficiency and economy. Before each experiment, the dye was added into the water and stirred together for 1 hour for well mixing.

Resazurin (resorufin)

Another dye used in this research is resazurin ($C_{12}H_6NNaO_4$, Sigma-Aldrich, USA, CAS: 62758-13-8). Resazurin is a phenoxazin-3-one dye which has been widely employed for testing bacterial or yeast contamination in biological fluids and milk, and also identifying the semen quality by colorimetry since the 1950s [60].

The dye solution is prepared with 100 $mg \cdot L^{-1}$ in the presence of sodium hydroxide (VWR, USA, CAS: 1310-73-2) and D-glucose anhydrous (Fischer Scientific, USA, CAS: 50-99-7), both diluted at 20 $g \cdot L^{-1}$. According to Anderson et al. [61], the reaction kinetics could be generally assumed to be the first-order dependence on the concentrations of glucose and resazurin, which means one mole of resorufin needs one mole of resazurin to be reduced with one mole of glucose. In our cases, the concentration of resazurin equals to 100 $mg \cdot L^{-1}$, namely 4.36×10^{-4} $mol \cdot L^{-1}$, thus the minimum concentration of glucose needs to be 7.86×10^{-2} $g \cdot L^{-1}$. For the minimum concentration of NaOH required, in fact, the first step of colorimetric reaction is the enolization of glucose by $[OH^-]$, then the glucose enediolate reduces resazurin to resorufin. However, unfortunately it is difficult to obtain the actual value of $[OH^-]$ by simply considering the quantity of NaOH used to prepare the solution. Therefore, we suggest the optimal employed concentrations of glucose and NaOH to be both 20 $g \cdot L^{-1}$, and the concentration of resazurin to be 0.1 $g \cdot L^{-1}$ to ensure the visualization and the post-treatment of the colored fields with a balance between the reaction kinetic rates and the requirement of adequate color intensity levels.

Under the applied concentration of the dye (with NaOH and Glucose), the corresponding enhancement factor equals to 1.03, which means that the enhancement effect of the colorimetric reaction on the mass transfer is negligible [45]. It should be noted that the presence of the dye had a small impact on the fluid property. Especially for cases with resazurin, the extra chemicals (NaOH and Glucose) slightly increased the viscosity of the liquid compared with the result measured in pure water.

As mentioned in section 1.3, the reduced resazurin, namely resorufin (pink), is highly fluorescent, which means it can play a role as an oxygen indicator. This feature makes it can be also used as a dye for PLIF technique.

3. VISUALIZATION RESULTS

With the experimental configuration, the mass transferred in the wake of the bubble could be visualized from two directions: side view and bottom view (see Figure 3).

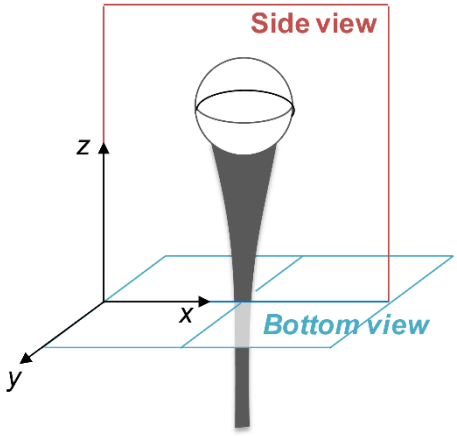

Figure 3 Schematic description of side view and bottom view for the mass transfer from the bubble

An example of images recorded by the three different visualization techniques from the side view are shown in Figure 4.

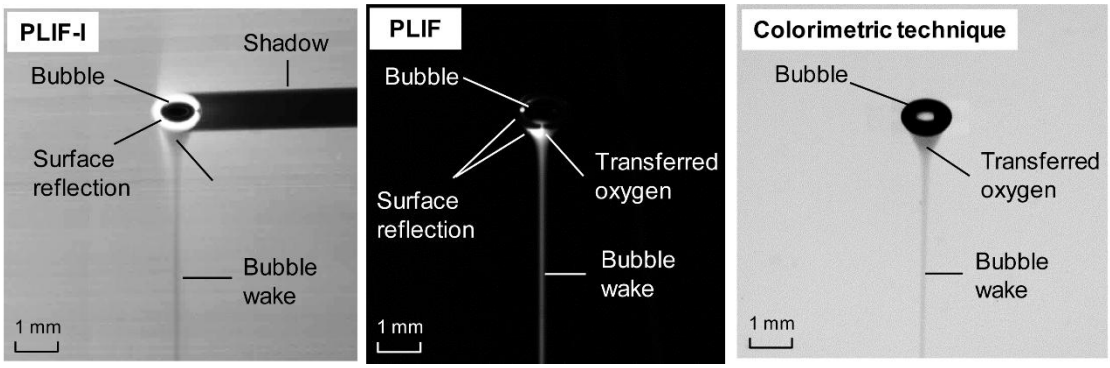

Figure 4 Recorded images from different visualization techniques (Side view)

On the image by PLIF-I and the colorimetric technique, the mass transfer zone is dark against a bright background, whereas the opposite is true for the images by PLIF. Some observations can be made:

(1) For the side view, the images using the laser techniques (PLIF or PLIF-I) suffer from a problem of reflection around the bubble surface.

(2) Regarding the bubble shadow on the PLIF-I image, a white ring appears around the bubble interface, making the bubble boundary difficult to recognize. Moreover, the reflection also has an impact on the mass transfer area near the bubble surface, especially for the part facing the laser (left part on the image). The effect diminishes along the laser direction but still cannot be neglected.

(3) For the PLIF image, the fluorescence effect is quite strong and the light around the bubble surface is relatively weaker than that in the bubble wake. Reflection occurs at the transfer interface, making the gray level recorded in this area much higher than the actually induced value.

(4) On the other hand, the local mass transfer by the colorimetric technique is quite clear, without the reflection issue. This property makes the colorimetric method suitable for tracking the mass transfer even near the gas-liquid interface.

(5) Far from the bubble surface, all three methods can visualize the mass transfer

346 properly.

347 Due to the reflection problem of the laser techniques, there is a lack of information
348 near the bubble surface, so it is difficult to precisely quantify the mass transfer with
349 side view images. By contrast, the absence of a reflection problem means that the
350 colorimetric technique can be used to calculate the mass transfer coefficient [42].

351

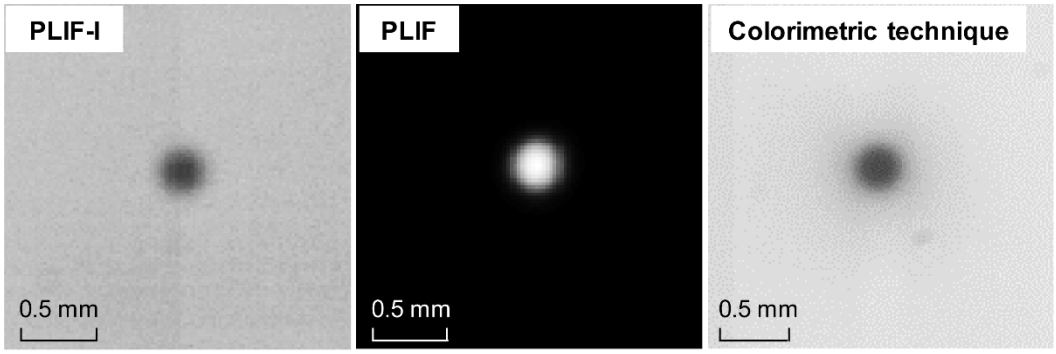

352

353 **Figure 5 Images recorded by different visualization techniques (bottom view)**

354

355 To avoid the reflection around the bubble caused by the laser flash, the camera is
356 placed under the column to record the mass transfer in one cross-section of the bubble
357 wake far from the passed bubble. From the bottom view, as shown in Figure 5, there
358 is good contrast between the mass transfer 'spot' and the background. The transferred
359 mass (dissolved oxygen) is concentrated at the spot center and becomes dispersed
360 near the boundary of the spot. Among the three images, the one by PLIF seems to
361 have the best quality, with the clear background (totally black) due to the different
362 color indicating mass transfer (white). The mass transfer can be quantified with
363 bottom view images for all three techniques.

364 **4. QUANTIFICATION OF MASS TRANSFER**

365 The relationship between the real oxygen concentration and the gray level recorded

on the images was established by the calibration process. Examples of the calibration results for the three techniques are shown in Figure 6. It can be seen that all three curves represent monotonic functions leading to a reasonable calculation of the oxygen concentration. The curve for PLIF is a straight line, showing that the gray level increase is directly proportional to higher oxygen concentration. For the other two curves (PLIF-I and colorimetric technique), the gray levels drop sharply, indicating that the dye is sensitive to low oxygen concentration ([O2] < 4 $mg \cdot L^{-1}$) but, when the oxygen concentration rises, the variation of the gray level is relatively small. For most of our cases, the oxygen concentration in the bubble wake was small within a reasonable calibration range.

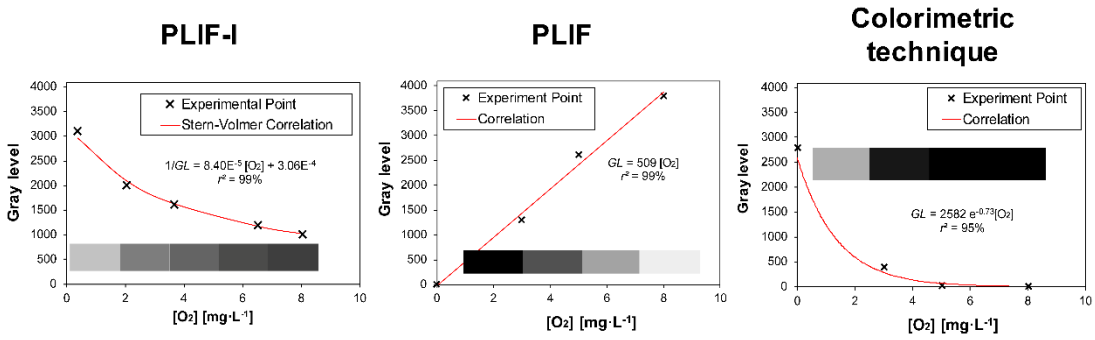

Figure 6 Examples of calibration result for three visualization techniques (PLIF-I, PLIF, and colorimetric technique).

Regarding the sensitivity of calibration, when dissolved oxygen concentration varies from 0 $mg \cdot L^{-1}$ to 8 $mg \cdot L^{-1}$, the change of gray levels for PLIF-I, PLIF, and the colorimetric technique is 2000, 4000 and 2500 respectively. Under the configuration investigated here, resorufin is more sensitive to the oxygen concentration when used as a fluorescent dye than when used as a colorimetric dye and is also better than the ruthenium complex. This property leads to better contrast between the transferred mass and the background, which will be discussed in the following sections.

In addition, unlike the results obtained in the microchannel [46], the calibration curve

of the colorimetric technique is not linear. That is because the thickness of the image area is no longer negligible when the camera takes images from the bottom of the column and the calibration is actually implemented within a volume instead of a thin plane. Thus, the Beer-Lambert absorption decreases the gray level, especially for the solutions with high concentrations of the dye.

With the calibration curve, the gray level expresses the oxygen concentration, and the concentration field of the dissolved oxygen in the bubble wake is plotted in Figure 7. It can be seen that the background noise on the PLIF image is less significant than in the other two images, which is consistent with the result for the side view in Figure 4. The background noise on the PLIF-I image is relatively significant, so a larger threshold is needed for PLIF-I to eliminate the impact of background noise.

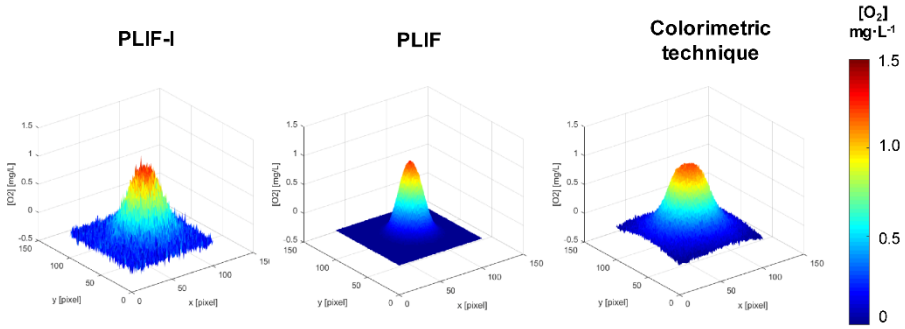

Figure 7 Examples of the dissolved oxygen concentration field in the bubble wake at the same moment (bottom view).

Unlike PLIF and PLIF-I techniques, the colorimetric technique gives a background concentration much higher than zero. It should be noted that the gray levels (mass transfer) recorded on the images by these three techniques are not exactly the same (see Figure 8). Since only a plane slice is lit by the laser sheet, the results by PLIF and PLIF-I display exactly the mass transfer in the cross-section concerned. For the colorimetric technique, the whole column is illuminated by the backlight and the

camera thus records the information not only in the focal plane but also in the front and the rear ones due to the depth of field. Its results refer to a superposition of the mass transfer in a series of continuous cross sections. This was probably the source of the deviation on the mass transfer estimation.

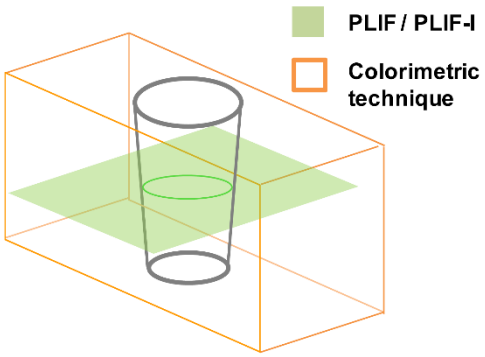

Figure 8 Image composition of mass transfer in bubble wake

In order to obtain the transferred mass flux, the image quality should be improved. An image processing procedure was implemented using Matlab (2017b) software. Firstly, the background impact was removed by subtracting the raw image from the average of 50 consecutive images just before the bubble went across the image plane. Then a threshold is applied to remove the remaining noise at the image background. A central region with resolution of 150×150 pixels was extracted which contained the mass transfer spot (see Figure 9 top). Since the spot had a circular distribution of the oxygen concentration that the oxygen diffused from the spot center to the surrounding, the extracted images of the oxygen field were then fitted with the 2D Gaussian diffusing model (see [35]), in which the oxygen concentration $[O_2]$ on the pixel (x, y) was estimated by:

$$[O_2]\,(x,y) = A\exp\frac{-(x-X)^2+(y-Y)^2}{B} \tag{5}$$

where A, B are the parameters representing the properties of a Gaussian distribution,

and (X,Y) is the center of the spot. These four parameters were determined by minimizing the error between the measured value $[O_2]$ and the value from the fitting model (Eq. (5)). The fitting images are shown in Figure 9 bottom.

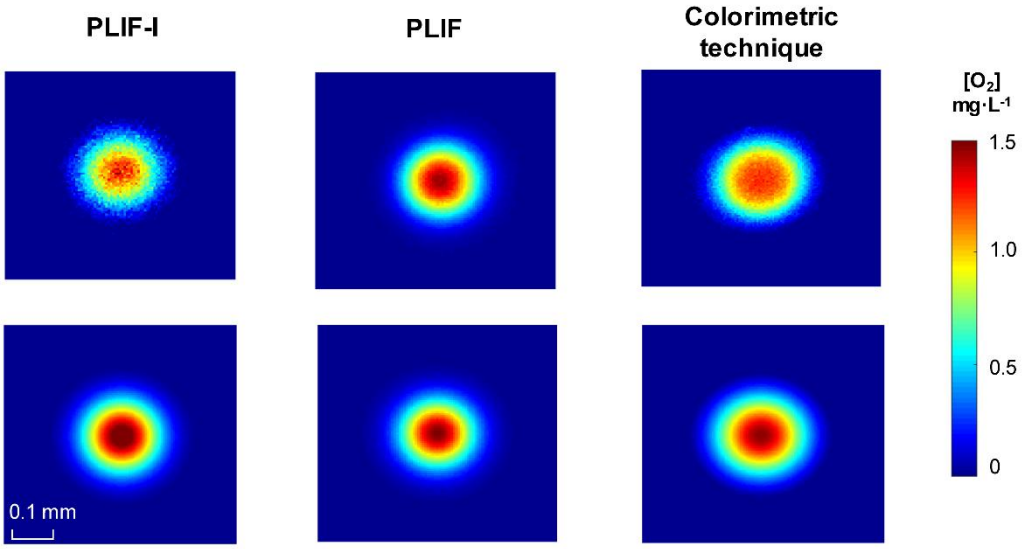

Figure 9 Corrected images (top) and fitted images (bottom) of the concentration field of dissolved oxygen in the bubble wake.

The fitting errors for all the three techniques are within 5%, validating the fitting Gaussian model. Summing the oxygen concentration in each pixel of the image area (see [62]) gives the fluxes before and after the fitting, as shown in Table 2. The PLIF technique has the best fitting result thanks to the good quality of its raw images.

Table 2 Result of fluxes before and after fitting for the three techniques

	Flux before fitting [mg·s^{-1}·m^{-2}]	Flux after fitting [mg·s^{-1}·m^{-2}]	Fitting error [%]
PLIF-I	3.53 ± 0.10	3.70	< 5%
PLIF	3.43 ± 0.03	3.45	< 1%
Colorimetric technique	3.35 ± 0.08	3.45	< 3%

The oxygen concentration field in the bubble wake was found for each recording moment (every 1/15 second) and the temporal evolution of the mass flux thus obtained is shown in Figure 10. For a small bubble with a linear trajectory, the mass transfer in the bubble wake far from the passed bubble is dominated by diffusion since the vertical convection induced by the bubble can be neglected. The mass transfer takes place by two-dimensional diffusion, which means that the total flux on the image should be conservative as a function of time.

It can be seen that, after the variation of the first several images due to the convection of the bubble, the fluxes measured by the three techniques tend to be constant versus time. For the PLIF and colorimetric cases, the fluxes are basically stable, but the total flux is slightly smaller than that found by PLIF-I. This flux decrease may be related to the presence of extra chemicals (NaOH and Glucose) impacting the liquid properties.

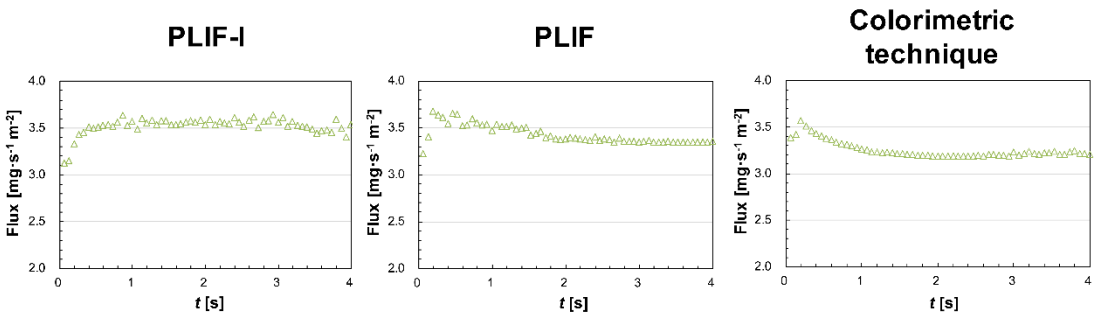

Figure 10 Mass flux versus time measured by different techniques (PLIF-I, PLIF, Colorimetric).

Plotting the fitted oxygen concentration along a line passing the spot center reveals that the distribution of the oxygen centration has a Gaussian profile. Based on this temporal evaluation of the oxygen profile in the bubble wake, it is possible to characterize the diffusion process (see Figure 11). It can be seen that the dissolved oxygen is concentrated at the spot center and then diffuses gradually to the surroundings, making the concentration over the area more homogeneous.

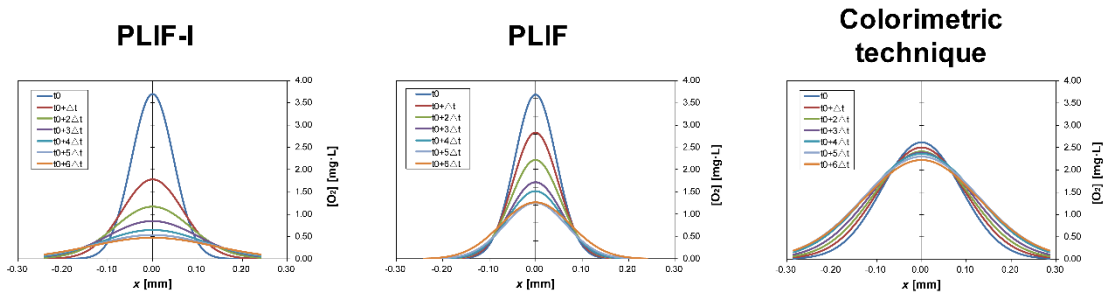

Figure 11 Temporal evolution of the O2 concentration field at the cross section of the bubble wake (left to right, results by PLIF-I, PLIF, and colorimetric technique. Δt= 0.67 s)

With the method introduced by Xu et al. [63], the area of the mass transfer spot expands as a function of time at a rate related to the diffusion coefficient:

$$S_{spot} = \pi R^2 = 2\pi Dt \tag{6}$$

The evolution of the spot area for the three techniques is plotted in Figure 12. For all three techniques, the curves of S_{spot} have good linearity versus time so the diffusion coefficient can be calculated from the slope of the curve (see Table 3).

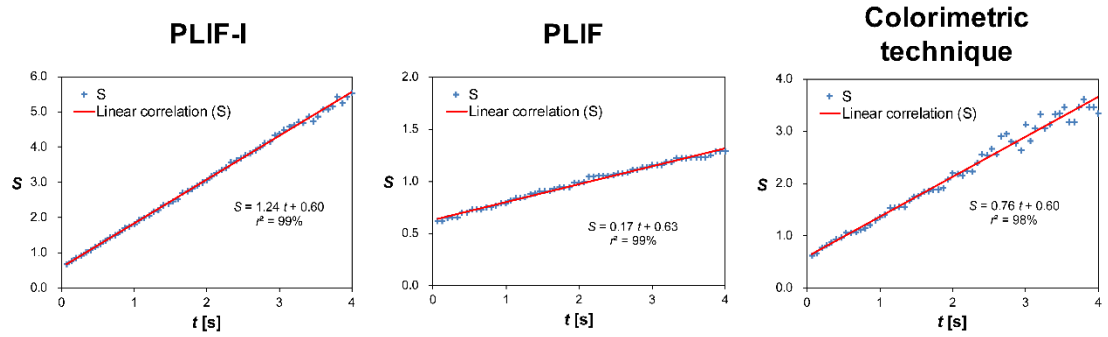

Figure 12 Evolution of the spot area as a function of time

Table 3 Diffusion coefficient results for the three techniques

	Slope of $S_{spot} - t$	r^2	D [$\times 10^{-9}$ m^2·s^{-1}]

PLIF-I	1.24	99%	1.97
PLIF	0.17	99%	0.27
Colorimetric	0.76	98%	1.20

The diffusion coefficients for the PLIF-I, PLIF and colorimetric techniques are 2×10^{-9} $m^2\cdot s^{-1}$, 0.27×10^{-9} $m^2\cdot s^{-1}$, and 1.20×10^{-9} $m^2\cdot s^{-1}$, respectively. In view of the technical problem mentioned above, the estimates of the diffusion coefficient using PLIF with resazurin and colorimetric technique are distorted. The reason is that these two techniques are based on the tracking of a different molecule (resorufin) rather than oxygen. The mathematical approach is based on the conservative flux, which may also contribute to the error for the result by PLIF with resazurin and the colorimetric technique. In contrast, the result by PLIF-I is consistent with the literature [30], proving more accurate for the quantification of the diffusion.

With the fluxes obtained from the images, the mass transfer coefficient can be estimated by dividing the flux J_{O_2} by the driving force. In our cases, the saturated concentration $[O_2]^*$ is close to 9 $mg\cdot L^{-1}$. For the PLIF-I technique, the bulk concentration $[O_2]_0$, measured after the deoxygenation of the liquid, is 0.2 $mg\cdot L^{-1}$. For the techniques with resazurin (PLIF and colorimetric technique), the oxygen is totally consumed or reacted before the experiment, so $[O_2]_0$ is assumed to be 0 $mg\cdot L^{-1}$.

$$k_L = \frac{J_{O_2}}{[O_2]^* - [O_2]_0} \tag{7}$$

The results for the mass transfer coefficients are given in Table 4. Regarding the underestimated flux, the value determined by the PLIF and colorimetric technique with resazurin is slightly smaller than that by PLIF-I. Nevertheless, all the values are consistent with the literature [64] indicating that all three techniques can be used for quantifying the mass transfer.

Table 4 Result of mass transfer coefficient by the three techniques

	k_L [$\times 10^{-4}$ m·s^{-1}]
PLIF-I	4.01 ± 0.010
PLIF	3.81 ± 0.005
Colorimetric technique	3.61 ± 0.008

5. DISCUSSION

The advantages and limitations of each technique are summarized in Table 5. All three techniques can be used for tracking the mass transfer to some extent. When resorufin (from resazurin) is used as a pink dye, the colorimetric technique can even visualize the mass transfer near the bubble surface. When it is used as a fluorescent dye, the image by PLIF technique shows good contrast between the mass transfer area and the pure black background. This property makes resorufin useful for the visualization of the mass transfer in a more complex structure induced by bigger bubbles (Figure 13). Since the resorufin has both pink color and fluorescence property, we can integrate the colorimetric and PLIF techniques by using the current experimental set-up (Figure 2). Based on the dual camera system, the mass transfer in both directions (side view and bottom view) can be visualized simultaneously. This would be a promising technique for the following study of local mass transfer characterization.

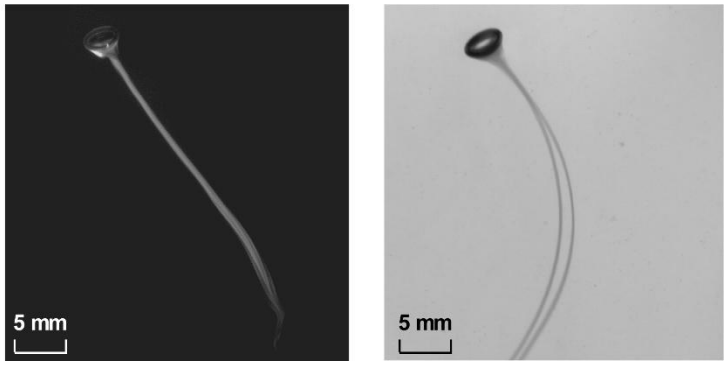

Figure 13 Visualization result with resorufin as a dye for bigger bubble (D_{eq}~3 mm). Left: image by PLIF; Right: image by colorimetric technique.

For the quantification of the mass transfer, the PLIF-I technique can give a reasonable result for the diffusion coefficient and mass transfer coefficient, while the other two techniques with resazurin do not correctly characterize the diffusion process due to the reaction mechanism. Another limitation for the PLIF and colorimetric techniques is that the oxygen indicator resazurin needs to be used together with extra chemicals (NaOH and glucose), which will have an impact on the fluid under investigation. The mass transfer coefficients measured by PLIF and coulometric techniques (with NaOH and glucose) remain in a reasonable range (3.6-3.8 $\times 10^{-4}$ m·s^{-1}), regardless a slight decrease compared to the PLIF-I technique (without NaOH and glucose). Thus, for our cases as oxygen mass transfer in deionized water, it has been proven that NaOH and glucose have no evident effect on mass transfer performance. However, it should be very careful when implement the colorimetric technique involving specific solute/solvent. The reaction possibility between the colorimetric solution and investigated solution should be carefully taken into account, which means NaOH and glucose, even resorufin could act as contaminants which affect mass transfer.

Table 5 Advantages and limitations of three techniques (PLIF-I, PLIF, colorimetric technique)

	Advantage ☑ or limitation ☒
PLIF-I	☑ Tracks mass transfer in the wake far from the surface ☑ Accurate quantification of flow flux ☑ Characterizes the diffusion ☒ Reflection at the bubble surface ☒ Significant background noise ☒ Shadow of the bubble
PLIF	☑ Tracks mass transfer in the wake far from the surface ☑ Less background noises ☒ Cannot characterize the diffusion of oxygen ☒ Reflection at the bubble surface ☒ Extra chemicals
Colorimetric technique	☑ Tracks mass transfer even near the bubble ☑ No reflection near the bubble ☒ Cannot characterize the diffusion of oxygen ☒ Complex composition of the recorded image ☒ Extra chemicals

CONCLUSIONS

Three different visualization techniques PLIF-I (with ruthenium complex), (PLIF (with fluorescent resorufin), and a colorimetric technique (with pink resorufin)) have been compared, with particular focus on their application to characterize the mass transfer around a single bubble rising in water. The PLIF and colorimetric technique with resazurin are both effective for tracking the local mass transfer. However, under our investigation conditions, there was a small distortion in the quantification of the

transferred oxygen fluxes by these two techniques, due to the presence of the extra chemicals (NaOH and Glucose). Moreover, they cannot be used to quantify the oxygen diffusive process as oxygen is consumed. Actually, these two techniques are based on the tracking of a different molecule (resorufin) instead of the oxygen molecule. Concerning the colorimetric technique, it is also less precise because its image contains the mass transfer not only on the target cross-section but also on those below and above it. Although the processing to remove the noise in the image background is relatively rigorous, PLIF-I is more accurate for the quantification of the diffusion coefficient and mass transfer coefficient.

NOMENCLATURE

Latin Symbols

C_{dye}	concentration of the dye
D	diffusion coefficient
F	fluorescence level
I	laser intensity
I_0	fluorescence intensities without quencher
I_Q	fluorescence intensities with quencher
J	Flux density
k_L	liquid side mass transfer coefficient
K_{SV}	Stern-Volmer constant
Q	concentration of the quencher molecule
r^2	determination coefficient
S_{spot}	area of mass transfer spot
t	time

ACKNOWLEDGMENTS

The financial assistance provided by the China Scholarship Council for Feishi XU is gratefully acknowledged. The federation Fermat is also thanked for its leading-edge material support.

REFERENCES

[1] K. Hanyu, T. Saito, Dynamical mass-transfer process of a CO2 bubble measured by using LIF/HPTS visualisation and photoelectric probing, Can. J. Chem. Eng. 88 (2010) 551–560. https://doi.org/10.1002/cjce.20319.

[2] P. Valiorgue, N. Souzy, M.E. Hajem, H.B. Hadid, S. Simoëns, Concentration measurement in the wake of a free rising bubble using planar laser-induced fluorescence (PLIF) with a calibration taking into account fluorescence extinction variations, Exp Fluids. 54 (2013) 1501. https://doi.org/10.1007/s00348-013-1501-y.

[3] C.R. Chu, G.H. Jirka, Turbulent gas flux measurements below the air-water interface of a grid-stirred tank, International Journal of Heat and Mass Transfer. 35 (1992) 1957–1968. https://doi.org/10.1016/0017-9310(92)90198-2.

[4] M. Riethues, R. Buchholz, U. Onken, H. Baumgärtl, D.W. Lübbers, Determination of oxygen transfer from single air bubbles to liquids by oxygen microelectrodes, Chemical Engineering and Processing: Process Intensification. 20 (1986) 331–337. https://doi.org/10.1016/0255-2701(86)80011-3.

[5] Herlina, G.H. Jirka, Application of LIF to investigate gas transfer near the air-water interface in a grid-stirred tank, Exp Fluids. 37 (2004) 341–349. https://doi.org/10.1007/s00348-004-0822-2.

[6] A. Charogiannis, J.S. An, C.N. Markides, A simultaneous planar laser-induced fluorescence, particle image velocimetry and particle tracking velocimetry technique for the investigation of thin liquid-film flows, Experimental Thermal and Fluid Science. 68 (2015) 516–536. https://doi.org/10.1016/j.expthermflusci.2015.06.008.

[7] R.K. Hanson, J.M. Seitzman, P.H. Paul, Planar laser-fluorescence imaging of combustion gases, Appl. Phys. B. 50 (1990) 441–454. https://doi.org/10.1007/BF00408770.

[8] J.P. Crimaldi, Planar laser induced fluorescence in aqueous flows, Exp Fluids. 44 (2008) 851–863. https://doi.org/10.1007/s00348-008-0496-2.

[9] K. Anderson, J.M. Cooper, S.J. Haswell, D. Marshall, H. Yin, X. Zhang, Microfluidic-based measurements of cytochrome P450 enzyme activity of primary mammalian hepatocytes, Analyst. 135 (2010) 1282–1287. https://doi.org/10.1039/C0AN00031K.

[10] H. Golnabi, M. Razani, Oxygen sensing based on the oxidation process in resorufin dye, Sensors and Actuators B: Chemical. 122 (2007) 109–117. https://doi.org/10.1016/j.snb.2006.05.012.

[11] M. Jimenez, N. Dietrich, G. Hébrard, Mass transfer in the wake of non-spherical air bubbles quantified by quenching of fluorescence, Chemical Engineering Science. 100 (2013) 160–171. https://doi.org/10.1016/j.ces.2013.01.036.

[12] P. Kováts, D. Thévenin, K. Zähringer, Investigation of Mass Transfer and Hydrodynamics in a Model Bubble Column, Chemical Engineering & Technology. 40 (2017) 1434–1444. https://doi.org/10.1002/ceat.201600679.

[13] J. Huang, T. Saito, Influence of Bubble-Surface Contamination on Instantaneous Mass Transfer, Chem. Eng. Technol. 38 (2015) 1947–1954. https://doi.org/10.1002/ceat.201500056.

[14] T. Lacassagne, M.E. Hajem, F. Morge, S. Simoens, J.-Y. Champagne, Study of Gas Liquid Mass Transfer in a Grid Stirred Tank, Oil Gas Sci. Technol. – Rev. IFP Energies Nouvelles. 72 (2017) 7. https://doi.org/10.2516/ogst/2017001.

[15] T. Lacassagne, S. Simoëns, M.E. Hajem, J.-Y. Champagne, Ratiometric, single-dye, pH-sensitive inhibited laser-induced fluorescence for the characterization of mixing and mass transfer, Exp Fluids. 59 (2018) 21. https://doi.org/10.1007/s00348-017-2475-y.

[16] S. Someya, S. Bando, Y. Song, B. Chen, M. Nishio, DeLIF measurement of pH distribution around dissolving CO2 droplet in high pressure vessel, International Journal of Heat and Mass Transfer. 48 (2005) 2508–2515. https://doi.org/10.1016/j.ijheatmasstransfer.2004.12.042.

[17] M.R. Eftink, Fluorescence Quenching Reactions, in: T.G. Dewey (Ed.), Biophysical and Biochemical Aspects of Fluorescence Spectroscopy, Springer US, Boston, MA, 1991: pp. 1–41. https://doi.org/10.1007/978-1-4757-9513-4_1.

[18] W.M. Vaughn, G. Weber, Oxygen quenching of pyrenebutyric acid fluorescence in water. Dynamic probe of the microenvironment, Biochemistry. 9 (1970) 464–473. https://doi.org/10.1021/bi00805a003.

[19] L.M. Wolff, Z.-C. Liu, T.J. Hanratty, A Fluorescence Technique to Measure Concentration Gradients near an Interface, in: ASCE, 1991: pp. 210–218. http://cedb.asce.org/cgi/WWWdisplay.cgi?73126 (accessed January 20, 2016).

[20] J. François, N. Dietrich, P. Guiraud, A. Cockx, Direct measurement of mass transfer around a single bubble by micro-PLIFI, Chem. Eng. Sci. 66 (2011) 3328–3338. https://doi.org/10.1016/j.ces.2011.01.049.

[21] V. Kapoustina, J. Ross-Jones, M. Hitschler, M. Raedle, J.-U. Repke, Direct spatiotemporally resolved fluorescence investigations of gas absorption and desorption in liquid film flows, Chem. Eng. Res. Des. 99 (2015) 248–255. https://doi.org/10.1016/j.cherd.2015.03.024.

[22] W.E. Asher, T.M. Litchendorf, Visualizing near-surface concentration

fluctuations using laser-induced fluorescence, Experiments in Fluids. 46 (2009) 243–253.

[23] P.M. Piccione, A.A. Rasheed, A. Quarmby, D. Dionisi, Direct Visualization of Scale-Up Effects on the Mass Transfer Coefficient through the “Blue Bottle” Reaction, J. Chem. Educ. 94 (2017) 726–729. https://doi.org/10.1021/acs.jchemed.6b00633.

[24] N. Dietrich, K. Loubière, M. Jimenez, G. Hébrard, C. Gourdon, A new direct technique for visualizing and measuring gas–liquid mass transfer around bubbles moving in a straight millimetric square channel, Chemical Engineering Science. 100 (2013) 172–182. https://doi.org/10.1016/j.ces.2013.03.041.

[25] W. Krieger, J. Lamsfuß, W. Zhang, N. Kockmann, Local Mass Transfer Phenomena and Chemical Selectivity of Gas-Liquid Reactions in Capillaries, Chemical Engineering & Technology. 40 (2017) 2134–2143. https://doi.org/10.1002/ceat.201700420.

[26] D. Colombet, D. Legendre, A. Cockx, P. Guiraud, F. Risso, C. Daniel, S. Galinat, Experimental study of mass transfer in a dense bubble swarm, Chemical Engineering Science. 66 (2011) 3432–3440. https://doi.org/10.1016/j.ces.2011.01.020.

[27] E. Bouche, S. Cazin, V. Roig, F. Risso, Mixing in a swarm of bubbles rising in a confined cell measured by mean of PLIF with two different dyes, Exp Fluids. 54 (2013) 1552. https://doi.org/10.1007/s00348-013-1552-0.

[28] M. Fedrizzi, J. Soria, Planar laser fluorescence imaging of bubble detachment, in: RMIT University, 2014: pp. 1–4.

[29] J. Moghaddas, C. Trägårdh, T. Kovacs, K. Östergren, A new method for measuring concentration of a fluorescent tracer in bubbly gas–liquid flows, Experiments in Fluids. 32 (2002) 728–729.

[30] U.D. Kück, M. Schlüter, N. Räbiger, Investigation on Reactive Mass Transfer at Freely Rising Gas Bubbles, in: Tampa, Florida, USA, 2010: pp. 1–5. http://ufdc.ufl.edu/UF00102023/00202 (accessed November 2, 2015).

[31] M. Stöhr, J. Schanze, A. Khalili, Visualization of gas–liquid mass transfer and wake structure of rising bubbles using pH-sensitive PLIF, Exp Fluids. 47 (2009) 135–143. https://doi.org/10.1007/s00348-009-0633-6.

[32] M. Yamamoto, M. Yamada, K. Morikawa, T. Sanada, T. Saito, Coupling mechanism between liquid phase motion and mass transfer around single rising bubbles by using PIV/LIF, in: Lisbon, Portugal, 2008.

[33] O. Bork, M. Schlueter, N. Raebiger, The Impact of Local Phenomena on Mass Transfer in Gas-Liquid Systems, Can. J. Chem. Eng. 83 (2005) 658–666.

https://doi.org/10.1002/cjce.5450830406.

[34] U.D. Kück, M. Schlüter, N. Räbiger, Local Measurement of Mass Transfer Rate of a Single Bubble with and without a Chemical Reaction, Journal of Chemical Engineering of Japan. 45 (2012) 708–712. https://doi.org/10.1252/jcej.12we059.

[35] N. Dietrich, J. Francois, M. Jimenez, A. Cockx, P. Guiraud, G. Hébrard, Fast measurements of the gas-liquid diffusion coefficient in the gaussian wake of a spherical bubble, Chem. Eng. Technol. 38 (2015) 941–946. https://doi.org/10.1002/ceat.201400471.

[36] T. Saito, M. Toriu, Effects of a bubble and the surrounding liquid motions on the instantaneous mass transfer across the gas–liquid interface, Chemical Engineering Journal. 265 (2015) 164–175. https://doi.org/10.1016/j.cej.2014.12.039.

[37] J. Huang, T. Saito, Discussion about the differences in mass transfer, bubble motion and surrounding liquid motion between a contaminated system and a clean system based on consideration of three-dimensional wake structure obtained from LIF visualization, Chemical Engineering Science. 170 (2017) 105–115. https://doi.org/10.1016/j.ces.2017.03.030.

[38] J. Huang, T. Saito, Influences of gas–liquid interface contamination on bubble motions, bubble wakes, and instantaneous mass transfer, Chemical Engineering Science. 157 (2017) 182–199. https://doi.org/10.1016/j.ces.2016.05.013.

[39] J. Timmermann, M. Hoffmann, M. Schlüter, Influence of Bubble Bouncing on Mass Transfer and Chemical Reaction, Chemical Engineering & Technology. 39 (2016) 1955–1962. https://doi.org/10.1002/ceat.201600299.

[40] M.W. Hlawitschka, P. Kováts, K. Zähringer, H.-J. Bart, Simulation and experimental validation of reactive bubble column reactors, Chemical Engineering Science. 170 (2017) 306–319. https://doi.org/10.1016/j.ces.2016.12.053.

[41] G. Kong, K.A. Buist, E.A.J.F. Peters, J.A.M. Kuipers, Dual emission LIF technique for pH and concentration field measurement around a rising bubble, Experimental Thermal and Fluid Science. 93 (2018) 186–194. https://doi.org/10.1016/j.expthermflusci.2017.12.032.

[42] N. Dietrich, G. Hébrard, Visualisation of gas-liquid mass transfer around a rising bubble in a quiescent liquid using an oxygen sensitive dye, Heat Mass Transfer. (2018) 1–9. https://doi.org/10.1007/s00231-018-2297-3.

[43] F. Xu, A. Cockx, G. Hébrard, N. Dietrich, Mass Transfer and Diffusion of a Single Bubble Rising in Polymer Solutions, Industrial & Engineering Chemistry Research. 57 (2018) 15181–15194. https://doi.org/10.1021/acs.iecr.8b03617.

[44] F. Xu, N. Midoux, H.-Z. Li, G. Hébrard, N. Dietrich, Characterization of bubble shapes in non-newtonian fluids by parametric equations, Chemical Engineering & Technology. 0 (2019). https://doi.org/10.1002/ceat.201800690.

[45] L. Yang, N. Dietrich, G. Hébrard, K. Loubière, C. Gourdon, Optical methods to investigate the enhancement factor of an oxygen-sensitive colorimetric reaction using microreactors, AIChE Journal. 63 (2017) 2272–2284. https://doi.org/10.1002/aic.15547.

[46] L. Yang, N. Dietrich, K. Loubière, C. Gourdon, G. Hébrard, Visualization and characterization of gas–liquid mass transfer around a Taylor bubble right after the formation stage in microreactors, Chemical Engineering Science. 143 (2016) 364–368. https://doi.org/10.1016/j.ces.2016.01.013.

[47] A. Kherbeche, J. Milnes, M. Jimenez, N. Dietrich, G. Hébrard, B. Lekhlif, Multi-scale analysis of the influence of physicochemical parameters on the hydrodynamic and gas–liquid mass transfer in gas/liquid/solid reactors, Chemical Engineering Science. 100 (2013) 515–528. https://doi.org/10.1016/j.ces.2013.06.025.

[48] A. Kherbeche, M. Mei, M.-J. Thoraval, G. Hébrard, N. Dietrich, Hydrodynamics and gas-liquid mass transfer around a confined sliding bubble, Chemical Engineering Journal. (2019). https://doi.org/10.1016/j.cej.2019.04.041.

[49] L. Yang, K. Loubière, N. Dietrich, C. Le Men, C. Gourdon, G. Hébrard, Local investigations on the gas-liquid mass transfer around Taylor bubbles flowing in a meandering millimetric square channel, Chemical Engineering Science. 165 (2017) 192–203. https://doi.org/10.1016/j.ces.2017.03.007.

[50] P. Kováts, D. Pohl, D. Thévenin, K. Zähringer, Optical determination of oxygen mass transfer in a helically-coiled pipe compared to a straight horizontal tube, Chemical Engineering Science. 190 (2018) 273–285. https://doi.org/10.1016/j.ces.2018.06.029.

[51] S. Kastens, J. Timmermann, F. Strassl, R.F. Rampmaier, A. Hoffmann, S. Herres-Pawlis, M. Schlüter, Test System for the Investigation of Reactive Taylor Bubbles, Chemical Engineering & Technology. 40 (2017) 1494–1501. https://doi.org/10.1002/ceat.201700047.

[52] C. Butler, E. Cid, A.-M. Billet, Modelling of mass transfer in Taylor flow: Investigation with the PLIF-I technique, Chemical Engineering Research and Design. 115 (2016) 292–302. https://doi.org/10.1016/j.cherd.2016.09.001.

[53] C. Butler, B. Lalanne, K. Sandmann, E. Cid, A.-M. Billet, Mass transfer in Taylor flow: Transfer rate modelling from measurements at the slug and film scale, International Journal of Multiphase Flow. 105 (2018) 185–201. https://doi.org/10.1016/j.ijmultiphaseflow.2018.04.005.

[54] E. Alméras, S. Cazin, V. Roig, F. Risso, F. Augier, C. Plais, Time-resolved measurement of concentration fluctuations in a confined bubbly flow by LIF, International Journal of Multiphase Flow. 83 (2016) 153–161. https://doi.org/10.1016/j.ijmultiphaseflow.2016.03.011.

[55] M. Roudet, A.-M. Billet, S. Cazin, F. Risso, V. Roig, Experimental investigation of interfacial mass transfer mechanisms for a confined high-reynolds-number bubble rising in a thin gap, AIChE J. 63 (2017) 2394–2408. https://doi.org/10.1002/aic.15562.

[56] F. Felis, N. Dietrich, A.-M. Billet, F. Strassl, S. Herres-Pawlis, V. Roig, K. Loubière, Experiments on reactive mass transfer around an oxygen bubble rising freely in a confined cell using colourimetric methods, in: Lisbon, Portugal, 2018: pp. 121–130.

[57] F. Felis, F. Strassl, L. Laurini, N. Dietrich, A.-M. Billet, V. Roig, S. Herres-Pawlis, K. Loubière, Using a bio-inspired copper complex to investigate reactive mass transfer around an oxygen bubble rising freely in a thin-gap cell, Chemical Engineering Science. (2019). https://doi.org/10.1016/j.ces.2019.07.045.

[58] S. Rüttinger, C. Spille, M. Hoffmann, M. Schlüter, Laser-Induced Fluorescence in Multiphase Systems, ChemBioEng Reviews. 5 (2018) 253–269. https://doi.org/10.1002/cben.201800005.

[59] M. Jimenez, Etude du transfert de matière gaz/liquide en milieux complexes: quantification du transfert d'oxygène par techniques optiques, INSA, 2013.

[60] R.E. Erb, M.H. Ehlers, Resazurin Reducing Time as an Indicator of Bovine Semen Fertilizing Capacity, Journal of Dairy Science. 33 (1950) 853–864. https://doi.org/10.3168/jds.S0022-0302(50)91981-3.

[61] L. Anderson, S.M. Wittkopp, C.J. Painter, J.J. Liegel, R. Schreiner, J.A. Bell, B.Z. Shakhashiri, What Is Happening When the Blue Bottle Bleaches: An Investigation of the Methylene Blue-Catalyzed Air Oxidation of Glucose, J. Chem. Educ. 89 (2012) 1425–1431. https://doi.org/10.1021/ed200511d.

[62] J. Francois, N. Dietrich, A. Cockx, A Novel Methodology to Measure Mass Transfer Around a Bubble, Mod. Phys. Lett. B. 25 (2011) 1993–2000. https://doi.org/10.1142/S0217984911027236.

[63] F. Xu, M. Jimenez, N. Dietrich, G. Hébrard, Fast determination of gas-liquid diffusion coefficient by an innovative double approach, Chemical Engineering Science. (2017). https://doi.org/10.1016/j.ces.2017.02.043.

[64] M. Roustan, Transferts gaz-liquide dans les procédés de traitement des eaux et des effluents gazeux, Tec & Doc Lavoisier, Paris; Londres; New York, 2003.

790

791